Frequency-Domain Interferometer for Measurement of the Group-Velocity Walkaway of Ultrashort Pulses in Birefringent Media

A new technique based on frequency-domain interferometry (FDI)[1,2] has been used to measure the group-velocity walkaway (GVW) of ultrashort pulses in birefringent media. As the name implies, this technique is based on the spectral interference of two short pulses in the frequency domain and makes use of the intrinsic phase delay between the fast and slow modes of a birefringent medium. Due to the different group delays, two pulses launched along the fast and slow axes will come out of the medium at different times. In the frequency domain, two temporally separated pulses interfere in the same way that two waves with different frequencies do in the time domain. In the frequency-domain interferometer described here, measurement of the modulation period of the interference fringes in the frequency domain gives the GVW directly without the need for further assumptions about the properties of the light source. By analogy with an ordinary interferometer, the two optical axes of the birefringent medium can be regarded as two interfering arms. A polarizer placed at the output end of the medium combines the two field components to generate interference fringes in the frequency domain. Temporally separated pulses can interfere owing to the linear dispersion of the grating in a spectrometer.[1,2] Different frequency components propagate along different directions, resulting in a frequency-dependent time delay. Therefore, two temporally separated pulses can physically overlap on the detector surface of the spectrometer. In comparison with other methods, the experimental setup of our interferometer is quite simple, and the alignment is very easy. Of greater significance is the fact that the experimental data is directly related to the GVW and no further curve fitting is needed.

To understand the physics of the frequency-domain interferometer, we must understand the properties of a spectrometer. A simplified version of a spectrometer is shown in Fig. 61.9. The incident beam is collimated and has a diameter D. The incident angle to the grating is i, while the diffracted angle is α. Assuming two pulses with pulse width τ_p that are separated by T, we find that the amplitude fronts of these two pulses are no longer parallel to the phase fronts after the grating. At the focus of the image lens, each pulse is temporally stretched to a duration of $DN\lambda/\cos(i)c$, where N is the groove number of the grating, λ is the wavelength of the pulses, and c is the speed of light. The two separate pulses can physically overlap for a time t_0 in at the focal (frequency) plane, provided that the original separation T is less than the grating-induced stretching $DN\lambda/\cos(i)c$ shown in Fig. 61.9.

FDI for the Measurement of Polarization Mode Dispersion of Single-Mode Optical Fibers

Single-mode optical fibers have seen increasing use in coherent optical transmission systems and as polarization-dependent fiber-optic sensors. A knowledge of the polarization properties of single-mode fibers is of fundamental importance in these applications since these properties govern the degree and state of the polarization of the radiation. It is well-known that birefringence in optical fibers can be induced by

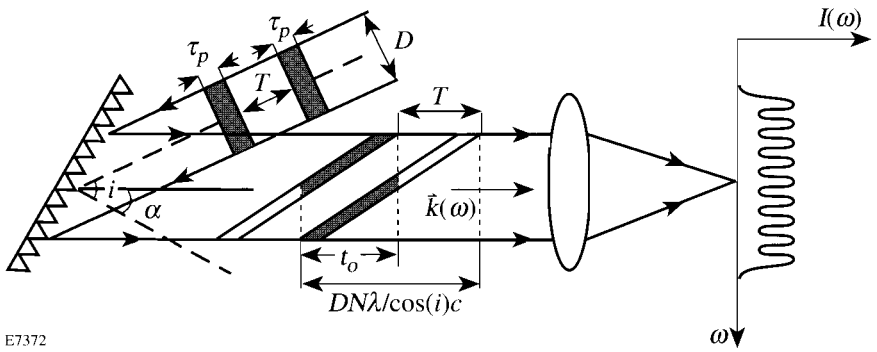

Figure 61.9
A simplified diagram illustrating temporal stretching of short pulses in a spectrometer. The incident angle to the grating is i; the diffracted angle is α.

built-in stress or by geometric deformation of the fiber core. The most important parameters characterizing birefringent fibers are the polarization mode dispersion (PMD) and modal birefringence (MB). Polarization mode dispersion is the group delay time difference between two orthogonally polarized HE_{11} modes, while modal birefringence is the refractive index difference between these two modes. In optical fiber communication systems, the presence of PMD results in bandwidth limitations.[3] Polarization mode dispersion has two contributions: one is the phase delay, which is proportional to modal birefringence; the other arises from dispersion difference between two modes. Since the first experimental verifications of PMD in birefringent optical fibers made by Rashleigh and Ulrich,[4] many methods for measuring PMD in single-mode fibers have been reported.[4–18] These methods fall into four categories: optical short-pulse methods,[7] frequency domain techniques,[8,9] interferometric methods,[4,8–16] and optical heterodyne techniques.[17–18] The white-light interferometric method has proved to be very accurate and applicable to meter-length samples.[4,16]

The configuration of the frequency-domain interferometer as used in our experiment is shown schematically in Fig. 61.10. The birefringent axes are labeled as x and y; the laser light propagates along the z direction. Two identical pulses temporally displaced by T are launched into the birefringent fiber with their polarization directions aligned to the x and y axes, respectively. At the input plane ($z = 0$), the electric fields of these two pulses can be expressed by

$$\begin{aligned} E_x(t, z=0) &= E(t)\exp(i\,\omega_0\,t) \\ E_y(t, z=0) &= E(t-T)\exp[i\,\omega_0(t-T)], \end{aligned} \tag{1}$$

where $E(t)$ is the slowly varying envelope of the two pulses and ω_0 is the carrier frequency of the laser pulses. At the exit end of the fiber, the Fourier transformations of the electric fields are

$$\begin{aligned} E_x(\omega, z=L) &= E(\omega-\omega_0)\exp[-i\,\beta_x(\omega)\,L] \\ E_y(\omega, z=L) &= E(\omega-\omega_0)\exp[-i\,\beta_y(\omega)\,L] \\ &\quad \times \exp(-i\,\omega\,T), \end{aligned} \tag{2}$$

where $E(\omega-\omega_0)$ is the Fourier transform of $E(t)$ and $\beta_x(\omega)$ and $\beta_y(\omega)$ are propagation constants of the x and y modes.

A polarizer with its transmission axis set to 45° with respect to the x and y axes combines the two electric fields:

$$E_{\text{out}}(\omega, z=L) = \frac{1}{2}\left[E_x(\omega, z=L) + E_y(\omega, z=L)\right]. \tag{3}$$

The power spectrum detected by a spectrometer can be expressed as

$$I(\omega) = \frac{1}{4}\left|E(\omega-\omega_0)\right|^2\left\{1+\cos[\Delta\beta(\omega)L+\omega T]\right\}, \tag{4}$$

where $\Delta\beta(\omega) = \beta_x(\omega) - \beta_y(\omega)$ is the modal birefringence and can be expanded as follows:

$$\begin{aligned} \Delta\beta(\omega) &= \Delta\beta(\omega_0) + \frac{d\Delta\beta(\omega_0)}{d\omega}\Delta\omega \\ &\quad + \frac{1}{2}\frac{d^2\Delta\beta(\omega_0)}{d\omega^2}\Delta\omega^2 + \ldots, \end{aligned} \tag{5}$$

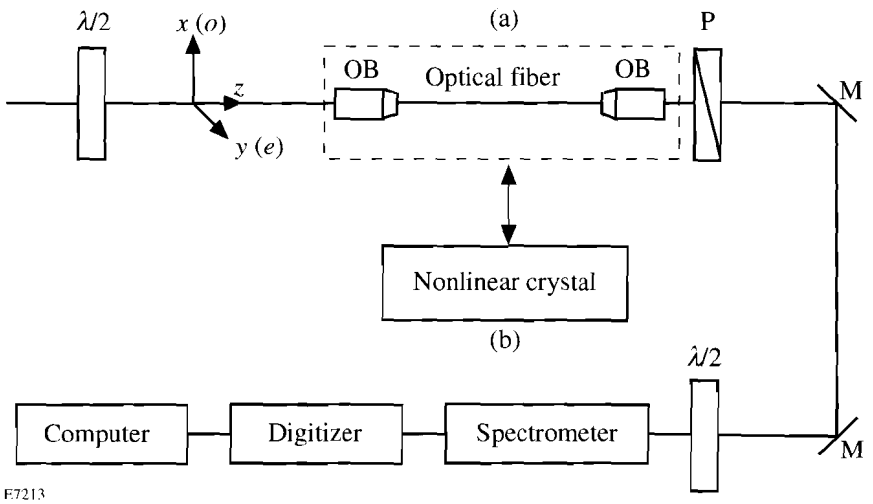

E7213

Figure 61.10
Experimental setup for measurement of GVW in birefringent media, where λ/2 = half-wave plate, OB = microscope objectives, P = polarizer, and M = mirror. Linearly polarized light is coupled into the birefringent sample with the polarization direction aligned 45° with respect to the optic axes. The microscope objectives and birefringent fiber (a) were replaced with CDA, KDP, or KD*P (b) for measurements of GVW in nonlinear crystalline media.

where $d\Delta\beta/d\omega$ is the polarization mode dispersion. The third term in Eq. (5) is the difference of group-velocity dispersion (GVD), which describes the difference in pulse spreading for the two principal axes. For subpicosecond pulses, the dispersion distance (the distance at which pulse width becomes twice the initial value) could be shorter than 1 m.[19] This term can be ignored, as pointed out in Ref. 4, since the difference in temporal spreading due to GVD is still negligible. Substituting Eq. (5) into Eq. (4) gives

$$I(\omega) = \frac{1}{4}\left|E(\omega-\omega_0)\right|^2 \times \left\{1+\cos\left[\Delta\beta(\omega_0)L+\frac{d\Delta\beta}{d\omega}\Delta\omega L+\omega T\right]\right\}. \quad (6)$$

From Eq. (6), the periodicity of the interference fringes is given by

$$\Omega = 2\pi\Big/\left(\frac{d\Delta\beta}{d\omega}L+T\right). \quad (7)$$

The polarization mode dispersion can be determined in terms of the measured quantity Ω, the fringe spacing in the frequency domain. From Eq. (7), we have

$$\frac{d\Delta\beta}{d\omega} = \left(\frac{2\pi}{\Omega}-T\right)\Big/L. \quad (8)$$

A careful examination of Eq. (8) reveals that there are two possible methods of measuring PMD. In the first method, no optical delay is needed ($T=0$), and a measurement of the fiber length L and interference spacing Ω gives the required result of PMD. This method has the advantage in that it is very simple to implement. The second method relies on adjustment of the temporal delay such that $\Omega=\infty$, which makes PMD $= -T/L$. Physically, this means that the predelay T is set so that two pulses come out of the fiber at the same time, resulting in no interference in the frequency domain.

The experimental setup is shown in Fig. 61.10. The laser beam originates from an actively mode-locked Nd:YLF oscillator that produces a 50-ps pulse train at a 1054-nm wavelength with a 100-MHz repetition rate. The pulse train goes through an 800-m, single-mode optical fiber that increases the bandwidth from 0.3 Å to 31.6 Å through the combined effects of self-phase-modulation (SPM) and GVD.[20] The pulses are then temporally compressed to 1 ps by a double-pass grating pair. Two microscope objectives are used to couple the laser beam into and out of a highly birefringent fiber (3M product, FS-HB-5651). A $\lambda/2$-wave plate placed in front of the fiber was used to control the polarization direction of the incident laser beam. A polarizer placed at the exit end of fiber was used to combine the electric field components of the fast and slow modes. Finally the collimated output beam was sent to a spectrometer equipped with an optical multichannel analyzer (OMA). Another $\lambda/2$-wave plate placed in front of the spectrometer was used to match the polarization direction of the laser beam to that of the grating inside the spectrometer. The waveguide parameters of the fiber used in the experiment are listed in Table 61.I.

Table 61.I: Waveguide parameters of the fiber used in the experiment.

Fiber length	2.750 m
Mode field diameter	6.8 μm
Fiber diameter	100 μm
Operating wavelength	1.060 μm
Cutoff wavelength	1.000 μm
Birefringence	4×10^{-4}
Loss	<2 dB/km

The input spectrum $\left[\left|E(\omega-\omega_0)\right|^2\right]$ is shown in Fig. 61.11. The power spectrum has nearly a square-top shape with a width of about 31.6 Å. In the experiment, the input polarization

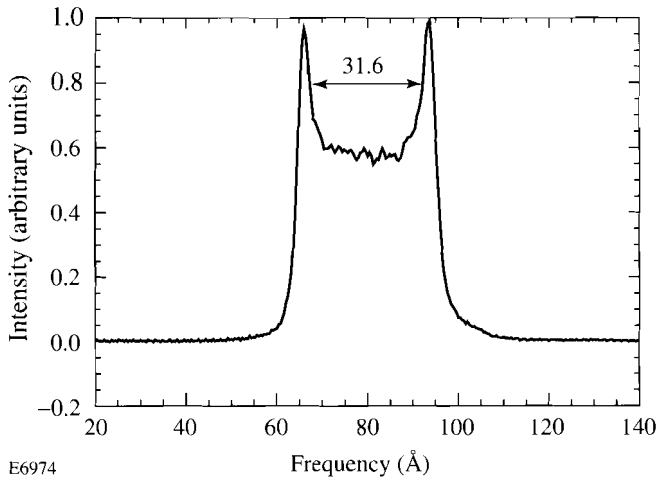

Figure 61.11
The spectrum of the incident pulses applied to the fiber. The spectrum shape is typical of the combined effects of SPM and GVD. The peak-peak width is 31.6 Å.

direction was adjusted to 45° with respect to the fast and slow axes of the birefringent fiber. The polarizer was also aligned to the same angle as described in Eq. (3). The frequency-domain interference fringes are shown in Fig. 61.12. The least-squares method was used to fit Fig. 61.12 using Eq. (6). The value of Ω was found to be 22.7±0.1 pixels, giving a modulational period of the interference fringes of 9.13±0.04 Å. The length of the fiber was measured to an accuracy of 1 mm. From Eq. (8), the PMD is found to be 1.42 ps/m with an accuracy of 1%. The term $d\Delta\beta/d\omega$ of Eq. (8) can also be expressed as

$$\frac{d\Delta\beta}{d\omega} = \frac{\Delta n}{c} + \frac{\omega}{c}\frac{d\Delta n}{d\omega}, \tag{9}$$

where Δn is the modal birefringence and c is the speed of light. Substituting the value for $\Delta\Omega$ from Table 61.I into Eq. (9) makes the first term on the right-hand side of Eq. (9) equal to 1.3±0.1 ps/m, which is very close to the measured PMD. The uncertainty comes from the fact that there is not enough information about the sample fiber. The contribution of the second term in Eq. (9) is much smaller than the first term, which is true in most stress-induced birefringent fibers.[20,21]

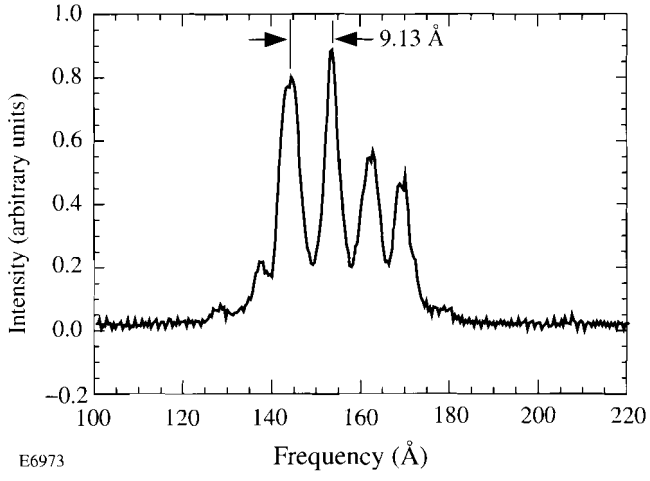

Figure 61.12
Frequency-domain interference fringes for the birefringent fiber. The fringe spacing is measured to be 9.13 Å.

FDI for the Measurement of GVW in Nonlinear Crystals

Frequency conversion in nonlinear crystals is an important method for obtaining coherent radiation sources for wavelengths not covered by lasers and is especially valuable in applications involving ultrashort laser pulses. Frequency conversion includes second (and higher) harmonic generation,[22–24] optical parametric oscillators (OPO), and optical parametric amplifiers (OPA).[25,26] A major limitation in ultrashort frequency conversion is the GVW between the ordinary (o-wave) and extraordinary (e-wave) waves due to the different group velocities for the two polarizations.[27] Since birefringence and dispersion exist in all nonlinear crystals, the GVW effect becomes a fundamental factor in determining the frequency-conversion efficiency. The walkaway has been used to increase the conversion efficiency in type-II doubling of 1-μm, 1-ps laser pulses by using a second crystal to predelay the extraordinary wave relative to the ordinary wave.[22,23] It was also found that the pulse duration could be reduced from 1 ps to 200 fs.[28] Chien *et al.*[24] have studied the conversion efficiency of high-power ultrashort pulses and have found that the GVW between two polarizations causes reconversion of the second harmonic back to the fundamental frequency.

The GVW between the e- and o-wave is of fundamental importance in the frequency conversion of ultrashort pulses. Typically, the walkaway is inferred by measuring the refractive indices and the dispersion of the e- and o-waves. Most values of the refractive index have been obtained by the minimum-deviation method (MDM) and are accurate to the fifth decimal place.[29] Extensive measurements of refractive indices of nonlinear crystals isomorphic to KH_2PO_4 have been made by Kirby and DeShazer.[30] Although MDM provides an accurate measurement of the refractive indices of e- and o-waves, it is not convenient for many applications involving nonlinear frequency conversion. Since the MDM measurement requires a high-quality prism made from the sample crystal, this method can be expensive and impractical for ordinary frequency-conversion applications. The dispersion properties are usually obtained by fitting to the Sellmeier or Zernike formula,[31,32] which requires multiple measurements with different light frequencies. Since narrow spectral lines of different lamps are used in MDM, it is possible that no experimental data exists for some specific wavelength that is used in frequency-conversion experiments. Another disadvantage of this method is that the refractive indices of o- and e-waves are a function of propagation direction. All calculations require that the locations of optical axes and the propagation angle, as well as the relative angle between the propagation direction and the optical axis, be known accurately.

In this section we report on an alternative method that allows direct measurement of the GVW between the e- and o-waves in a birefringent crystal. There are several other advantages of this technique as far as nonlinear frequency conversion is concerned. In practical applications of frequency

conversion involving short pulses, it is desirable to know the walkaway parameter for the laser frequency involved. Since the walkaway can be measured using the same laser pulses that will be used in frequency conversion, the measured data about the walkaway is immediately relevant. For the applications involving cascade processes of frequency conversion of short pulses, it is crucial to know either the polarization direction or the crystal orientation that corresponds to the minimum walkaway, so that the orientations of nonlinear crystal for the next stage of frequency conversion can be optimized.[28] To our knowledge, this method provides the first direct measurement of angular dependence of the GVW.

From Eq. (4), the power spectrum detected in the spectrometer takes the following form:

$$I(\omega) = \frac{1}{4}\left|E(\omega - \omega_0)\right|^2 \left[1 + \cos(\phi_0 + \Delta\tau\Delta\omega)\right], \qquad (10)$$

where $E(\omega - \omega_0)$ is the spectrum of the incident pulse, ϕ_0 is a constant, $\Delta\tau$ is the temporal delay between the two pulses traveling along the fast and slow axes of the crystal, and $\Delta\omega = \omega - \omega_0$. The GVW is therefore equivalent to the periodicity of the interference pattern in the frequency domain.

The experimental setup is as shown in Fig. 61.10, except that the birefringent fiber and microscope objectives used for in-and-out coupling the incident light are replaced by a nonlinear crystal. The frequency-domain interference fringes for a 2.5-cm-thick CDA crystal are shown in Fig. 61.13. A least-squares method is used to fit Fig. 61.13 using Eq. (10), as shown by the dashed curve. There are three sources of error in the measurements: (1) measuring the length of the crystal, (2) calibrating the spectrometer, and (3) determining the spacing of the interference fringes. The error bar for thickness measurement is 1%. The calibration was performed using five spectral lines of a rubidium lamp ranging from 1053 nm to 1073 nm. The spectral lines were fitted with a Lorentzian line shape, and the overall error bar in the calibration was found to be 0.2%. The least-squares fit for the interference fringes gave an error of 0.3%. The largest source of error is in the measurement of the crystals' thickness. After taking into account these three error sources, we found that the error in determining the temporal walkaway is about 1%. The experimentally determined GVW values for several commonly used nonlinear crystals are listed in Table 61.II, along with the cut angles and lengths of the tested crystals. The last column of Table 61.II shows the calculated values of the GVW based on the dispersion data of Ref. 30; the measured results are very close to the calculated ones. As mentioned previously, this method can also be used to measure the length of a birefringent crystal if its GVW parameter is known. The last row of Table 61.II shows the length of a KDP-I crystal determined by this method using the calculated result of the walkaway; the resolution is about 50 μm.

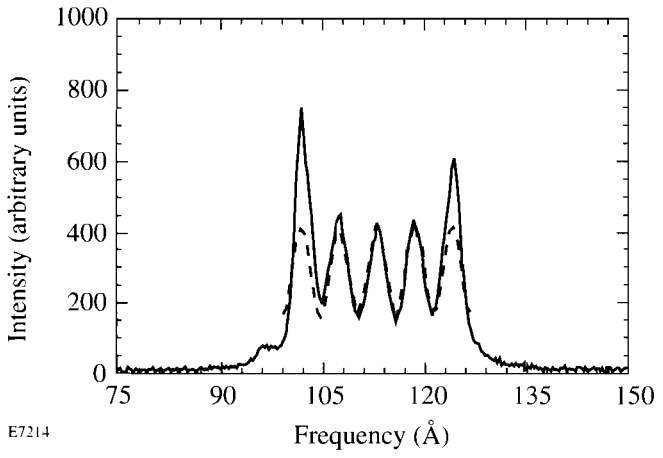

Figure 61.13
Frequency-domain interference fringes of the CDA-I sample. The fringe spacing is measured to be 6.7 Å. The solid line is the experimental data, while the dashed line is the theoretical fitting.

Table 61.II: Parameters of nonlinear crystals and measured walkaway.

Crystal	Cut angle	Length ×2 (cm)	Walkaway [(a)] (ps/cm)	Walkaway [(b)] (ps/cm)
CDA I	85.0°	2.50	1.00±0.01	1.01
KDP* II	53.7°	1.50	0.94±0.02	0.97
KDP II	59.2°	1.90	1.35±0.02	1.33
KDP I	41.2°	1.029±0.005	–	0.79

(a) Measured results
(b) Calculated results

Since the refractive index of the extraordinary wave is a function of propagation direction, the GVW will also be affected by the direction of propagation, as shown by the plot of walkaway dependence versus propagation angle in Fig. 61.14. The angle is measured with respect to the phase-matching angle of the crystal (KDP-II) in the YZ plane. The scattered triangles are experimental data, while the solid curve is the theoretical prediction based on the material dispersion.[24] The experimental data fits the theory very well, with an accuracy of 1%. The angle shown in Fig. 61.14 is the angle inside the crystal as obtained by Snell's law. The propagation

distance is also a function of angle due to the cube-shaped crystal, which has been taken into account in Fig. 61.14. In our experiment, the pulses were not transform limited (i.e., the pulses are slightly chirped). It is believed that the chirp may be responsible for the finite visibility of the interference patterns, which could affect the accuracy of the measurements when visibility is poor.

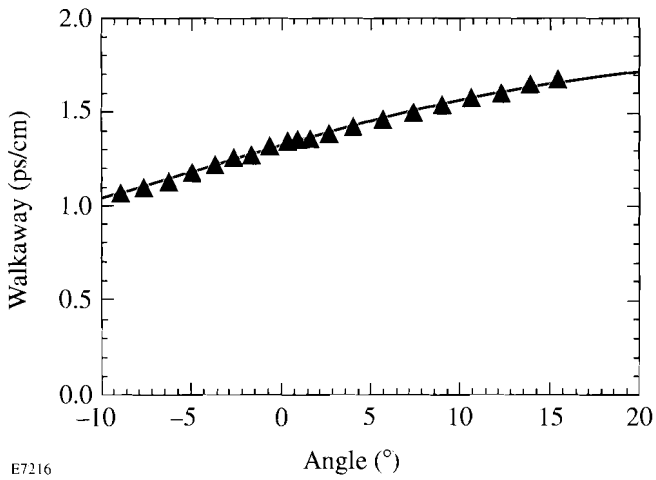

Figure 61.14
Dependence of the group-velocity walkaway on the propagation direction. The angle is measured with respect to the phase-matching angle of the sample (KDP-II).

Conclusions

A new technique based on frequency-domain interferometry has been used to measure the polarization mode dispersion of birefringent media. In contrast to the usual interferometric methods that measure the interference visibility as a function of optical delay between two interfering arms, we measure the periodicity of the interference fringes in the frequency domain by using short, broadband optical pulses. No curve fitting is needed to find the values of PMD since the measured modulation period of the fringes is directly related to PMD. Two schemes of measurement, differing only in the requirements for an optical delay line, have been presented, and one method (without the delay line) was demonstrated experimentally. Advantages of this new method include (1) direct, real-time measurement of the group-velocity walkaway, which is useful for applications in which the GVW can be controlled by tuning the crystals; (2) values of GVW at the appropriate wavelength for most frequency-conversion applications since the source is the same as that used in the nonlinear frequency conversion; and (3) determination of the angular dependence of GVW, which is useful for experiments involving serial frequency conversion in that the walkaway can be compensated for in the second crystal.[28] Compared to other methods, the frequency-domain interferometric technique provides reasonably good accuracy, experimental simplicity, and linearity in the sense that it is not dependent on the laser power.

ACKNOWLEDGMENTS

This work was supported by the U.S. Department of Energy, Office of Inertial Confinement Fusion under Cooperative Agreement No. DE-FC03-92SF19460, the University of Rochester, and the New York State Energy Research and Development Authority. The support of DOE does not constitute an endorsement by DOE of the views expressed in this article.

REFERENCES

1. N. F. Scherer *et al.*, J. Chem. Phys. **95**, 1487 (1991).
2. E. Tokunaga, A. Terasaki, and T. Kobayashi, Opt. Lett. **17**, 1131 (1992).
3. I. P. Kaminow, IEEE J. Quantum Electron. **QE-17**, 15 (1981).
4. S. C. Rashleigh and R. Ulrich, Opt. Lett. **3**, 60 (1978).
5. Y. Sasaki, N. Shibata, and J. Noda, Electron. Lett. **18**, 997 (1982).
6. M. Monerie, P. Lamouler, and L. Jeunhomme, Electron. Lett. **16**, 907 (1980).
7. Y. Yamabayashi and M. Saruwatari, Electron. Lett. **19**, 239 (1983).
8. K. Mochizuki, Y. Namihira, and H. Wakabayashi, Electron. Lett. **17**, 153 (1981).
9. N. Shibata, M. Tateda, and S. Seikai, IEEE J. Quantum Electron. **QE-18**, 53 (1982).
10. N. Imoto and M. Ikeda, IEEE J. Quantum Electron. **QE-17**, 542 (1981).
11. S. C. Rashleigh, Opt. Lett. **7**, 294 (1982).
12. S. C. Rashleigh, *ibid.* **8**, 336 (1983).
13. A. B. Grudinin, G. L. Dyankov, and V. B. Neustruev, Sov. J. Quantum Electron. **16**, 1522 (1986).
14. L. Thévenaz, V. de Coulon, and J.-P. Von der Weid, Opt. Lett. **12**, 619 (1987).
15. J.-P. Von der Weid, L. Thévenaz, and J.-P. Pellaux, Electron. Lett. **23**, 151 (1987).
16. W. J. Bock and W. Urbanczyk, Appl. Opt. **32**, 5841 (1993).
17. N. Shibata, M. Tsubokawa, and S. Seikai, Electron. Lett. **20**, 1055(1984).
18. N. Shibata, M. Tsubokawa, and S. Seikai, Opt. Lett. **10**, 92 (1985).
19. G. P. Agrawal, *Nonlinear Fiber Optics* (Academic, Boston, 1989), Chaps. 3–5.
20. N. K. Sinha, Phys. Chem. Glasses **18**, 66 (1978).

21. N. Shibata *et al.*, J. Opt. Soc. Am. **73**, 1972 (1983).

22. Y. Wang and R. Dragila, Phys. Rev. A **41**, 5645 (1990).

23. Y. Wang, B. Luther-Davis, Y.-H. Chuang, R. S. Craxton, and D. D. Meyerhofer, Opt. Lett. **16**, 1862 (1991).

24. C. Y. Chien, G. Korn, J. S. Coe, J. Squier, G. Mourou, and R. S. Craxton, submitted to Optics Letters.

25. R. L. Byer, J. Opt. Soc. Am. B **10**, 1656 (1993).

26. R. L. Byer, *ibid.* **10**, 2148 (1993).

27. R. W. Boyd, *Nonlinear Optics* (Academic Press, San Diego, 1992).

28. Y. Wang and B. Luther-Davies, Opt. Lett. **17**, 1459 (1992).

29. W. L. Wolfe, "Properties of Optical Materials," in *Handbook of Optics*, edited by W. G. Driscoll (McGraw-Hill, 1978), Sec. 7, pp. 7-1–7-157.

30. K. W. Kirby and L. G. DeShazer, J. Opt. Soc. Am. B **4**, 1072 (1987).

31. M. Born and E. Wolf, *Principles of Optics*, 6th ed. (Pergamon, Oxford, 1986).

32. F. Nernike, Jr., J. Opt. Soc. Am. **54**, 1215 (1964).